# Indirect Band Gaps in Quantum Dots Made from Direct-Gap Bulk Materials

A.J. WILLIAMSON, A. FRANCESCHETTI, H. FU, L.W. WANG, and ALEX ZUNGER

National Renewable Energy Laboratory, Golden, CO 80401

The conditions under which the band gaps of free standing and embedded semiconductor quantum dots are direct or indirect are discussed. Semiconductor quantum dots are classified into three categories; (i) free standing dots, (ii) dots embedded in a direct gap matrix, and (iii) dots embedded in an indirect gap matrix. For each category, qualitative predictions are first discussed, followed by the results of both recent experiments and state of the art pseudopotential calculations. We show that:

- Free standing dots of InP, InAs, and CdSe will remain direct for all sizes, while dots made of GaAs and InSb will turn indirect below a critical size.
- Dots embedded within a direct gap matrix material will either stay direct (InAs/GaAs at zero pressure) or will become indirect at a critical size (InSb/InP).
- Dots embedded within an indirect gap matrix material will exhibit a transition to indirect gap for sufficiently small dots (GaAs/AlAs and InP/GaP quantum well) or will be always indirect (InP/GaP dots, InAs/GaAs above 43 kbar pressure and GeSi/Si dots).

In indirect nanostructures, charge separation can occur with electrons and holes localized on different materials (flat InP/GaP quantum well) or with electrons and holes localized in different layers of the same material (concentric cylindrical GaAs/AlAs layers).

**Key words:** Heterostructures, nanostructures, quantum dots

## INTRODUCTION

One of the most important properties used to classify the optical response of a quantum dot system is whether it has a direct or indirect band gap. In dots with *direct gaps*, the electron and hole wavefunctions are both confined within the dot and are both derived from the Brillouin zone center $\Gamma$ states. This produces strong oscillator strengths for optical transitions and a strong luminescence. Dots with *indirect band gaps* can be indirect in real space, in which case the electrons and holes are localized in different regions of the nanostructure (e.g., dot interior vs barrier), and/or indirect in reciprocal space, where the states involved in the optical transitions evolve from different **k** points in the Brillouin zone. The oscillator strengths for optical transitions in dots with indirect gaps are small, producing weak luminescence.

There are several physical factors which control whether the interband transitions in a quantum dot will be direct or indirect: As a starting point, one has to consider the order of the levels (e.g., $\Gamma_{1c}$ and $X_{1c}$) in the bulk material from which the dot is derived. Does the bulk material have a direct (InP, GaAs) or indirect (GaP, Si) gap and what is the spacing of the levels? On moving from a bulk system to a dot system, the level ordering can be dramatically altered by the effects of (i) quantum confinement which drives electron levels up in energy and hole levels down in energy in inverse proportion to their respective effect masses, and (ii) strain, which can drive levels either up or down in energy depending on the sign of the deformation potential. Finally, if the quantum dot is embedded within a matrix of another semiconductor such as "self-assembled" dots grown by the Stranski Krastanow (SK)[1] technique,[2–4] the energy levels in the matrix material have to be considered along with the dot energy levels. If the lowest electron level in the barrier is below that of the dot, then electrons may localize in the barrier, producing a system that is indirect in real space. Similarly, if the highest hole level in the barrier is above that of the dot, then holes

(Received September 18, 1998; accepted January 9, 1999)

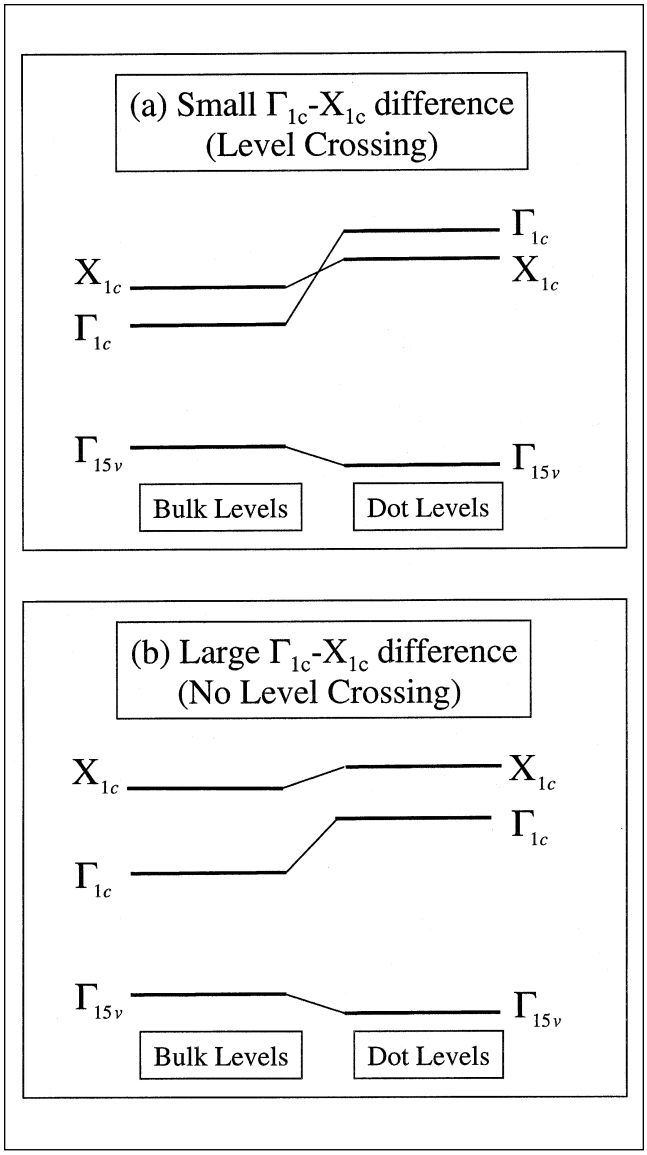


Fig. 1. Schematic illustration of the change in energy level order as a result of quantum confinement in free standing quantum dots.

may localize in the barrier, again producing a system that is indirect in real space.

In this paper, we consider the question of when a dot or nanostructure made of a direct gap bulk material such as GaAs, InP, InAs, or InSb will remain direct or switch to an indirect band gap. We classify quantum dot systems into three specific categories:

- Free standing dots (i.e., dots without a barrier), e.g., InP, InAs, InSb, and GaAs. We will predict that GaAs dots become indirect below a given size, while InAs stays direct for all sizes. Also under pressure, free standing InP dots become indirect at a lower pressure than the bulk.
- Dots embedded within a *direct* gap barrier material, e.g., InSb/InP[5] and InAs/GaAs.[3,4] We will predict that InAs/GaAs stays direct, while InSb/InP becomes indirect.
- Dots embedded within an *indirect* gap barrier material, e.g., InP/GaP,[2] GeSe/Si,[6] GaAs/AlAs,[7] and InAs/GaP.[8,9] We will predict that for sufficiently small dots, GaAs/AlAs becomes indirect, while InP/GaP and GeSi/Si are indirect for all sizes.

We discuss the physical factors that determine the above behavior and present theoretical predictions of where any crossovers may take place. Where available, we summarize recent experimental results.

## FREE STANDING QUANTUM DOTS

Colloidal chemistry techniques have been successfully used to synthesize free standing quantum dots made from InP,[10] CdSe,[11] InAs,[12] and CdS.[13] For each of these materials, high quality samples, with narrow size distributions (<5%) have been produced. The surfaces of the dots are passivated by a combination of organic molecules and HF treatments. After such treatments, the dots can produce quantum yields as high as 60%.[10] These free standing dots are considered strain free.

When predicting whether the band gap of free standing quantum dots is direct or indirect, there are two factors to consider:

- The initial level ordering in the bulk material from which the dot is derived, and
- The size of the quantum dot and the resulting quantum confinement.

### Qualitative Expectations

On moving from the bulk to a quantum dot, translational symmetry is broken, and **k** is no longer a good quantum number. However, analysis of quantum dot wavefunctions shows that they are constructed from a packet of states in reciprocal space centered on a specific point in the Brillouin zone of the parent bulk material, such as the Γ, X, or L points. In the following discussion, we shall refer to states constructed from states around the Γ point as "Γ derived," and similarly for X and L points. To obtain a rough idea of whether the $\Gamma_{1c}$, and $X_{1c}$ derived quantum dot levels from a bulk material with a direct gap will cross each other producing a system with a gap that is indirect in reciprocal space, we consider the predictions of effective mass theory. The energies of the $\Gamma_{1c}$ and $X_{1c}$ derived energy levels of a dot with radius R are given by

$$\varepsilon_{\Gamma_{1c}}(R) = \varepsilon_{\Gamma_{1c}}(\infty) + \frac{\hbar^2\pi^2}{2m_\Gamma^* R^2}$$
$$\varepsilon_{X_{1c}}(R) = \varepsilon_{X_{1c}}(\infty) + \frac{\hbar^2\pi^2}{2m_X^* R^2}, \quad (1)$$

where $\varepsilon_{\Gamma_{1c}}(\infty)$ and $\varepsilon_{X_{1c}}(\infty)$ are the bulk energies of the respective conduction bands and $m_\Gamma^*$ and $m_X^*$ are the effective masses of electrons at the Γ and X points. The energy difference between the dot X and Γ levels is therefore given by

$$\varepsilon_{X_{1c}}(R) - \varepsilon_{\Gamma_{1c}}(R) = \left[\varepsilon_{X_{1c}} - \varepsilon_{\Gamma_{1c}}\right]_{bulk} + \frac{A}{R^2}\left[\frac{1}{m_X^*} - \frac{1}{m_\Gamma^*}\right]. \quad (2)$$

**Table I. Experimentally Measured Values[14] for the Position of the $\Gamma_{1c}$ and $X_{1c}$ Levels with Respect to Each Materials Valence Band Maximum**

| Material | $\Gamma_{1c}$ | $X_{1c}$ | $\Gamma_{1c} - X_{1c}$ | $m^*_{\Gamma_{1c}}$ | $m^*_{X_{1c}}$ |
|---|---|---|---|---|---|
| InAs | 0.37 | 2.28 | 1.91 | 0.02 | 2.0 |
| InSb | 0.25 | 1.71 | 1.46 | 0.01 | 2.0 |
| InP | 1.50 | 2.44 | 0.94 | 0.08 | 2.05 |
| GaAs | 1.51 | 2.03 | 0.52 | 0.07 | 1.18 |
| AlAs | 2.79 | 2.37 | –0.42 | 0.18 | 1.56 |

Crossing will therefore occur if (i) the initial energy difference, $\left[\varepsilon_{X_{1c}} - \varepsilon_{\Gamma_{1c}}\right]_{bulk}$, is not too large, and (ii) the $\Gamma$ mass, $m^*_\Gamma$, is sufficiently lighter than the X mass, $m^*_X$. Figure 1a shows schematically the energy levels of a quantum dot constructed from a direct gap bulk material with a small $\Gamma_{1c} - X_{1c}$ spacing in the conduction band. Quantum confinement in the dot drives the $\Gamma_{1c}$ level above the $X_{1c}$ level, producing a dot with an indirect gap. Figure 1b shows the opposite situation where there is a large $\Gamma_{1c} - X_{1c}$ spacing in the conduction band. Quantum confinement effects in this dot are not sufficient to drive the $\Gamma_{1c}$ level above the $X_{1c}$ level, hence the dot will have a direct gap. The experimentally measured[14] bulk energy level spacings and the electron effective masses of InAs, InSb, InP, GaAs, and AlAs are given in Table I. Figure 2 shows the initial bulk $\Gamma_{1c} - X_{1c}$ spacing vs the difference between the effective mass predictions for the quantum confinements [from Eq. (1)] of the $\Gamma_{1c}$ and the $X_{1c}$ levels for quantum dots constructed from each of these materials. A line is drawn for each material, whose endpoints correspond to the difference between the quantum confinement of the $\Gamma_{1c}$ and $X_{1c}$ levels for dots with radii of 30 and 100Å, calculated using the simple effective mass expression in Eq. (1). The figure is divided into two regions by the thick diagonal line. Dots falling to the left of the line have a larger initial $\Gamma - X$ spacing than quantum confinement difference, and hence have a direct band gap. For the dots on the right of the line, the effects of quantum confinement cause a level crossing and hence an indirect band gap. Figure 2 predicts that InAs and InP dots will remain direct, even when their radius is reduced to 30Å, whereas InSb and GaAs will undergo a direct to indirect transition at a sufficiently small radius. As bulk AlAs has an indirect gap, AlAs dots of all sizes will also have an indirect gap. Of course, the effective mass theory described in Eq. (1) is only qualitative, so we next describe realistic calculations of the effects.

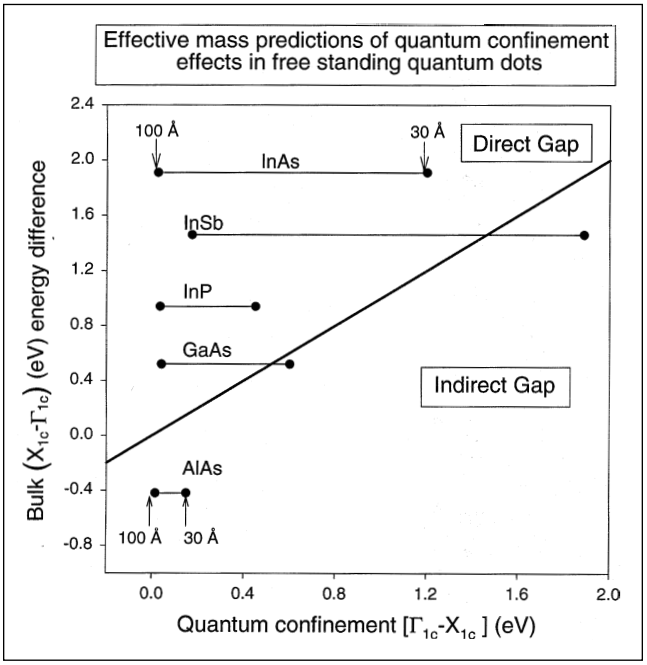


Fig. 2. The bulk $\Gamma_{1c} - X_{1c}$ spacing vs the difference between the effective mass estimated [Eq. (1)] quantum confinement of the $\Gamma_{1c}$ and the $X_{1c}$ levels for AlAs, GaAs, InP, InAs, and InSb quantum dots. For each material, the endpoints of the line correspond to the difference between the quantum confinement of the $\Gamma_{1c}$ and $X_{1c}$ levels for dots with radii of 30 and 100Å, calculated using Eq. (1).

## Calculations

Our method of calculation is based on the use of a single particle empirical pseudopotential Hamiltonian,

$$\hat{H} = -\frac{1}{2}\nabla^2 + \sum_{\alpha,n} \upsilon_\alpha\left(\mathbf{r} - \mathbf{R}_{\alpha n}\right) + \upsilon_\alpha^{(SO)}. \qquad (3)$$

The potential describing the quantum dot system is constructed from a sum of screened atomic pseudopotentials, $\upsilon_\alpha$, where $\alpha$ represents the different atomic species and $\mathbf{R}_{\alpha n}$ are the positions of all the atoms within the dot and barrier materials. The pseudopotentials, $\upsilon_\alpha$, have been fitted[15] to the experimental band gaps, effective masses and deformation potentials of the bulk binary materials. We use the reciprocal space functional form of the pseudopotential from Ref. 15.

$$\upsilon_\alpha(\mathbf{q}) = \left[1 + a_{4\alpha}\mathrm{Tr}(\varepsilon)\right] a_{0\alpha} \frac{\left(q^2 - a_{1\alpha}\right)}{a_{2\alpha} e^{a_{3\alpha} q^2} - 1}, \qquad (4)$$

where $a_{0\alpha}$, $a_{1\alpha}$, $a_{2\alpha}$, $a_{3\alpha}$, $a_{4\alpha}$ are adjustable parameters[15] and $\mathrm{Tr}(\varepsilon)$ is the trace of the strain tensor.[16] We assume the bulk zinc-blende structure and use the bulk interatomic spacings obtained from experiment.[14]

We expand the single particle wavefunctions, $\psi_i$, in a plane wave basis

$$\psi_i(\mathbf{r}) = \sum_{G}^{E_{cut}} V_{G,i}\ e^{iG.r} \qquad (5)$$

The, matrix elements of the Hamiltonian in Eq. (3) in the basis of Eq. (5) are calculated according to

$$\hat{H}_{G,G'} = \frac{1}{2}G^2 \ \delta_{G,G'} + V_{local}(G-G') + V_{nonlocal}(G-G') \quad (6)$$

The spin orbit interaction is represented by a nonlocal pseudopotential, $\upsilon_\alpha^{(SO)}$, which is evaluated in real space using the linearly scaling small box method from Ref. 17.

The quantum dots, surrounded by either vacuum or a barrier material, form a supercell which is periodically repeated. Sufficient vacuum/barrier material is used, to ensure that the interactions between each dot and its periodic images are negligible. These supercells contain up to one million atoms, which is too large for the Hamiltonian in Eq. (3) to be solved by conventional diagonalization methods. We thus use the "folded spectrum method" (FSM),[18,19] in which one solves for the eigenstates of the equation

$$\left(\hat{H} - \varepsilon_{ref}\right)^2 \psi_i = \left(\varepsilon - \varepsilon_{ref}\right)^2 \psi_i, \quad (7)$$

where $\varepsilon_{ref}$ is a reference energy. By placing $\varepsilon_{ref}$ within the gap, and close to the valence band maximum or conduction band minimum, one is then able to obtain the top few valence states or the bottom few conduction states, respectively.

Note that this empirical pseudopotential approach to the single-particle problem includes shape effects, interface effects and spin-orbit coupling in the Hamiltonian [Eq. (3)]. However, it neglects self-consistency, which is expected to produce a negligible effect in such large quantum dots.

*Direct Gap Dots: InP, InAs, and CdSe*

The simple qualitative ideas expressed in the section "Free Standing Quantum Dots: Qualitative Expectations" were tested using the pseudopotential methods described above for a number of free standing quantum dots including GaAs,[20,21] InP,[22–26] InAs,[27] and CdSe.[28,29] For InP, InAs, and CdSe, it was found that the bulk spacing between the $\Gamma_{1c}$ level and the next lowest level in the conduction band is sufficiently large (see Table I) that the effects of quantum confinement do not cause the dots to develop an indirect band gap, even for dots as small as 20Å radius. There are several recent experiments[11,22–28,30] which clearly show the existence of a direct band gap in free standing InP,[31] InAs,[12] and CdSe[11] quantum dots. These experiments observe a strong fundamental photoluminescence (PL) peak that blue shifts as the size of the dots decreases which is interpreted as evidence for a direct band gap in these dots.

*Quantum Confinement Induced Direct to Indirect Crossover: GaAs*

In the case of free standing GaAs nanostructures, pseudopotential calculations[20,21] on dots, wires, and films predict there is a critical size below which the band gap will be indirect as a result of the quantum confinement effects illustrated in Fig. 1 and Fig. 2. These critical sizes are given in the first line of Table II. Figure 3 shows the CBM energies of a series of GaAs films and wires varying in thickness/diameter from 1 to 25 monolayers. The electron states derived from the $\Gamma_{1c}$ and $X_{1c}$ states have different effective masses and therefore have different quantum confinement energies. This produces a $\Gamma_{1c} \rightarrow X_{1c}$ crossing at a critical film thickness of approximately ten monolayers and a critical wire diameter of approximately 15 monolayers. Figure 4 shows a plot of the CBM wavefunction amplitude in a cross-sectional plane through two free standing GaAs quantum wires, one with a diameter less than the critical size and one

**Table II. Critical Sizes (in ML) for the Direct/ Indirect Crossover in Free-Standing GaAs Quantum Films, Wires, and Dots[20]**

| | Film | Wire | Dot |
|---|---|---|---|
| Free-standing | 8 | 14 | >15 |
| AlAs embedded | 13 | 25 | >15 |

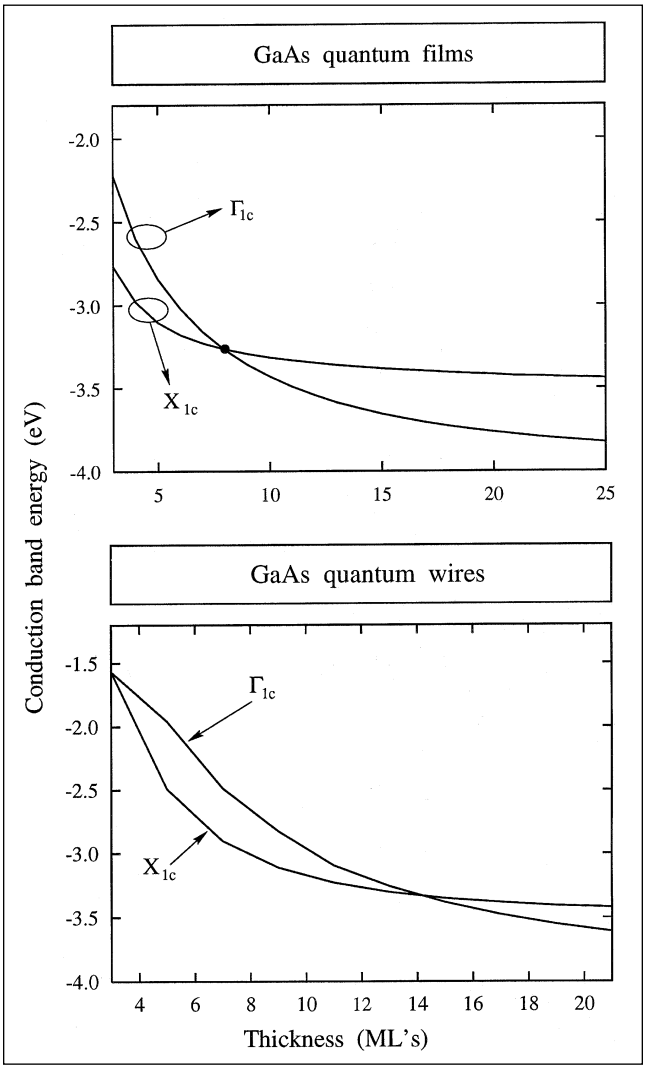


Fig. 3. Pseudopotential calculation of $\Gamma_{1c}$ and $X_{1c}$ energies of free-standing, hydrogen-passivated GaAs $(1\,\bar{1}\,0)$ quantum films and $(1\,\bar{1}\,0) \times (110)$ quantum wires as a function of the thickness/diameter (in MLs).[21]

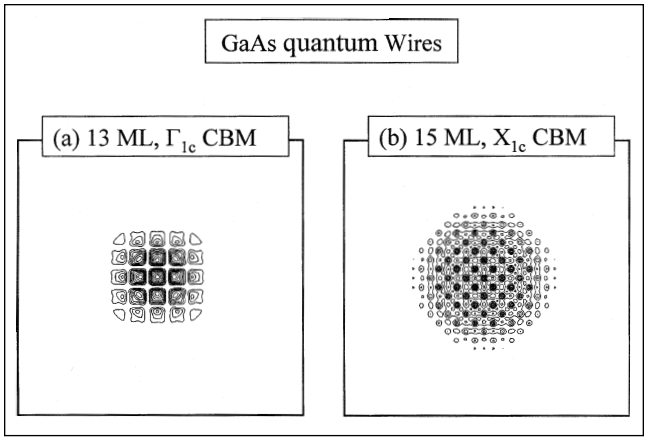


Fig. 4. Amplitude of the CBM wavefunctions in a cross-sectional plane through two free standing GaAs quantum wires, one with a diameter less than the critical size for the Γ – X crossover (13 ML) and one larger (15 ML) than the critical size.[21] Note the $\Gamma_{1c}$ and $X_{1c}$ wavefunction character in (a) vs (b).

larger than the critical size. Although both wavefunctions are strongly localized within the wire, it is clear that the Bloch function corresponding to the $X_{1c}$ derived CBM in the smaller wire has a different symmetry to that corresponding to the $\Gamma_{1c}$ derived state in the larger wire. So far there has been no experimental testing of the predicted[20,21] direct-indirect transition in free standing GaAs quantum nanostructures, presumably because the methods that produce free standing dots (e.g., colloidal chemistry[10]) have not yet been perfected for GaAs.

*Pressure Induced Direct to Indirect Crossover: InP*

In quantum dot systems, structural phase transitions usually occur at increased pressures compared to the bulk. For example the transition to the β-Sn structure in Si nanocrystals.[32] However, recent calculations of InP dots under hydrostatic pressure[26] show that the reduced dimensionality acts to *reduce* the pressure at which the band gap switches from direct to indirect. The lighter effective mass at the $\Gamma_{1c}$ point ($0.08m_0$) compared to $X_{1c}$ point ($2.05m_0$) produces much stronger quantum confinement effects for electrons whose wavefunctions are derived from the Γ point. This difference in quantum confinement reduces the $\Gamma_{1c} - X_{1c}$ separation in the zero pressure quantum dot relative to the bulk. The pressure required to induce a direct to indirect band gap transition is therefore also decreased in dots compared to that in bulk. For example, calculations[26] predict a relative deformation Δa/a of 0.0414 is required to produce a level crossing in bulk InP, compared to Δa/a of 0.0245 in a InP quantum dot with a diameter of 34.8Å.

## DOTS EMBEDDED WITHIN A DIRECT GAP BARRIER MATERIAL

### Qualitative Expectations

When a quantum dot is embedded within a matrix of another material, two factors in addition to quantum confinement can affect whether the band gap of the dot is direct or indirect. Firstly, if the band offsets between the dot and matrix have a type II alignment, with the conduction band minimum of the matrix below that of the dot, this alone can produce a band gap that is indirect in real space, with electrons localized in the barrier. Secondly, if there is a lattice mismatch between the dot and the matrix, the coherent heterostructure system will be strained. The strain profile couples to the band offsets via the deformation potentials of the individual bands and can change a system that has a type I alignment in the absence of strain to an indirect type II alignment in the presence of strain, and hence an indirect band gap.

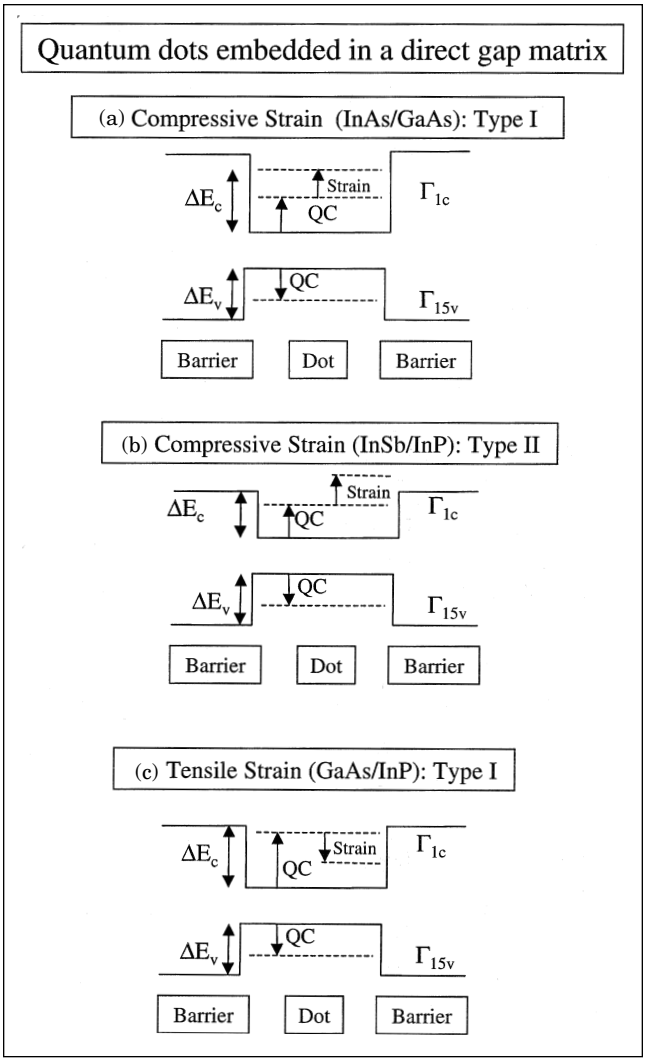


Fig. 5. Schematic illustration of the band alignment for quantum dots constructed from a direct gap material embedded within a matrix with a direct band gap. The bulk band energies are shown with solid lines and the confined electron and hole levels are shown by dashed lines. The conduction and valence band offsets are marked as $\Delta E_c$ and $\Delta E_v$. The energetic effects of quantum confinement (QC) and strain are illustrated by the arrows.

This is illustrated in Fig. 5. Quantum confinement (QC) pushes electron levels up and hole levels down. The effect of strain is as follows. The dot states derived from the $\Gamma_{1c}$ conduction state have a strongly *positive* deformation potential (e.g., for GaAs $a_{\Gamma_{1c}}$

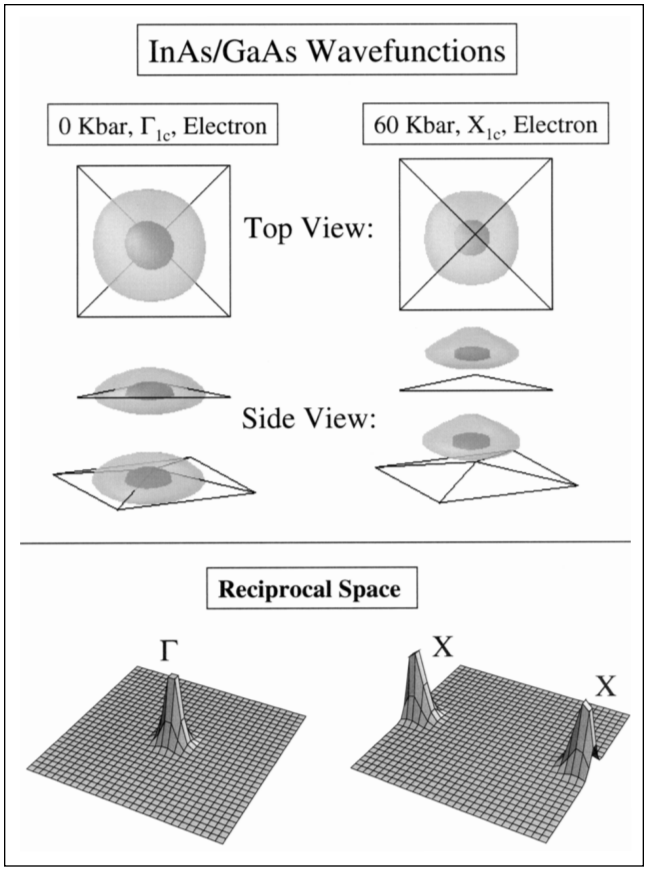


Fig. 6. Calculated[33] wavefunctions squared of a pyramidal InAs dot, (base = 100Å, height = 10Å) embedded in GaAs, at zero and 60 kbar hydrostatic pressure. In real space isosurfaces are shown at 25% (light) and 75% (dark) of the maximum value. In reciprocal space, the momentum space projection in the $k_y = 0$ plane of the zinc-blende Brillouin zone are shown. At zero pressure, both electron and hole wavefunction are localized in the InAs quantum dot, whereas above the transition pressure the electrons are localized in a strain induced pocket above the quantum dot.

~10.7 meV/kbar$^{-1}$) , and hence move up in energy in response to compression (InAs in GaAs, Fig. 5a and InSb in InP Fig. 5b), and down in response to tensile strain (GaAs in InP) Fig. 5c). Valence states derived from the $\Gamma_{15v}$ point typically have a small positive deformation potential (e.g., for GaAs $a_{\Gamma_{15v}}$ ~1.7 meV kbar$^{-1}$) and therefore move less under strain. If a dot embedded in a matrix with a direct gap is compressed as a result of strain (InSb in InP), this can push the $\Gamma_{1c}$ level in the dot toward that of the matrix thus approaching a type II alignment (GaAs in InP, Fig. 5c). The key quantity which controls whether dots in such a system have a direct or indirect band gap is the conduction band offset, $\Delta E_c$, which measures the difference between the bulk energies of the lowest conduction band in the dot and the embedding matrix. If the natural (unstrained, no quantum confinement) value of $\Delta E_c$ is large enough (e.g., InAs/GaAs), then the effects of strain and quantum confinement will not be able to overcome it and the dots will always have a direct band gap. However, if $\Delta E_c$ is small then the effects of strain and quantum confinement (InSb/InP) could push the energy of the $\Gamma_{1c}$ level in the dot above that of the embedding matrix, producing a system that has an indirect gap in real space.

Finally, if the initial $\Gamma_{1c} - X_{1c}$, conduction band level spacing in the quantum dot material is small (e.g., GaSb) then the larger quantum confinement of $\Gamma_{1c}$ derived states compared to $L_{1c}$ derived states resulting from the lighter effective mass at the Γ point may alone be sufficient to produce an embedded dot with a band gap that is indirect in reciprocal space. Such a crossover has already been observed in GaSb/AlSb quantum wells. Similar quantum dot experiments need to be performed.

## Calculations

### *Direct Gap Dots: InAs / GaAs*

The most common example of quantum dots embedded within a direct gap matrice is that of InAs dots embedded within a GaAs matrix. Using the Stranski-Krastanow growth technique, this system has been shown[3,4] to produce high quality quantum dots with a relatively small size distribution. In the InAs/GaAs system, the conduction band offset, $\Delta E_c$ is large (1.05 eV), and spectroscopic measurements agree with pseudopotential calculations[33–35] that strain effects and quantum confinement are not large enough to

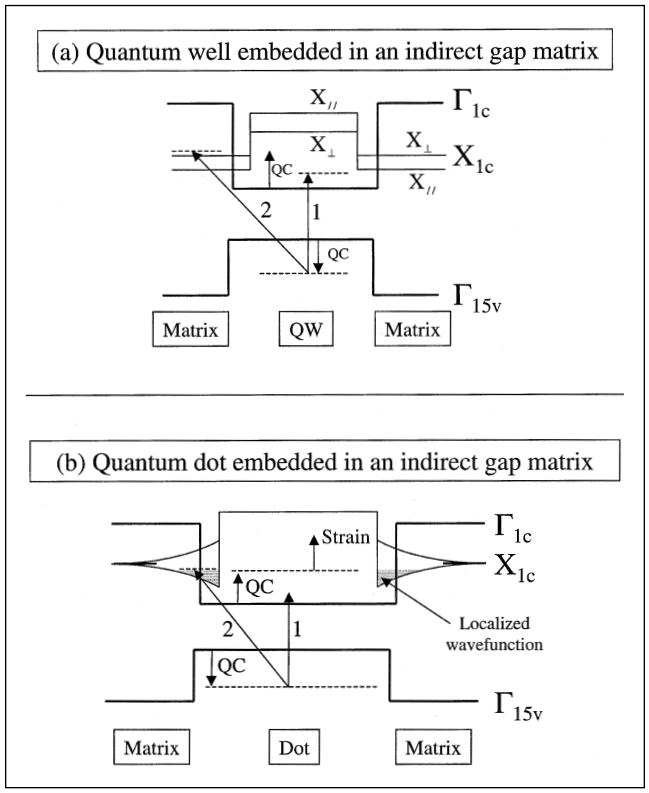


Fig. 7. Schematic illustration of the band alignment for quantum wells and dots constructed from a direct gap material embedded within a matrix with an indirect band gap. The bulk band energies are shown with solid lines and the confined electron and hole levels are shown by dashed lines. The effect of strain induced splitting of the $X_{1c}$ points is shown. Excitations corresponding to direct and indirect transitions are shown by arrows 1 and 2. Quantum confinement effects are indicated by the arrows marked QC.

convert the InAs to an indirect dot. This is illustrated on the left hand side of Fig. 6 which shows an isosurface plot of the lowest energy electron state at zero pressure. It shows that the state is localized within the InAs pyramidal dot, i.e., the band gap is direct in real space. The bottom of Fig. 6 shows the same state in reciprocal space. This state is derived from the Γ point in the bulk band structure, i.e., the band gap is direct in reciprocal space. We expect that GaAs/InP dots will also remain direct, as explained in Fig. 5c.

*Indirect Gap Dots: InSb/InP*

In contrast to the InAs/GaAs system, the InSb/InP system has a very small conduction band offset, $\Delta E_c$. Recently, Prieto et al.[5] predicted this offset to be as small as 0.05 eV and they showed that if uncapped InSb dots are grown on an InP substrate the band alignment is type I, and the dots have a direct band gap. However, if these dots are capped with another InP layer, the InP capping layer compresses the InSb dots. This compressive strain raises the energy of the $\Gamma_{1c}$ level in the InSb dots with respect to the $\Gamma_{1c}$ level in the InP matrix. For InSb dots smaller than 10 ML, the combination of quantum confinement and the strain induced raising of the $\Gamma_{1c}$ level produces a type II band alignment (Fig. 5b), and hence InSb dots with a band gap that is indirect in real space.

*Quantum Confinement Induced Direct to Indirect Transition: GaSb/AlSb*

GaSb is only barely a direct gap semiconductor: the L valley is approximately 85 meV above Γ valley. The effective mass of electrons in the L valley is about ten times higher[14] than that in the Γ valley. For quantum wells with a width less the 40Å, quantum confinement effects have been shown[36] to push the Γ derived states above the energy of the L derived states, producing a system with a band gap that is indirect in reciprocal space. To date, no such observations have been made for GaSb/AlSb quantum *dots*.

## DOTS EMBEDDED WITHIN AN INDIRECT GAP BARRIER MATERIAL

### Qualitative Expectations

When a quantum well or dot constructed from a direct gap material is embedded in a barrier material with an indirect gap, one has to consider the effects of strain and quantum confinement on both the Γ derived states and the off-Γ derived states (such as X and L) in *both* the dot/well material and the barrier material.

If the dot/well and barrier are lattice matched, e.g., GaAs/AlAs, one only has to consider the effects of quantum confinement when calculating whether a particular system has a direct or indirect gap. Figure 7a shows the band alignments for a quantum well constructed from a direct gap material embedded in an indirect gap barrier. The band alignment is type I, with both electrons and holes localized in the quantum well. However, the $X_{1c}$ level in the barrier is not too far above the $\Gamma_{1c}$ level in the well. For a wide quantum well, the quantum confinement effects will be small and the system will have a direct gap (see arrow 1 in Fig. 7a). When the well gets narrower, quantum confinement effects could push this $\Gamma_{1c}$ derived state confined in the well, above the energy of the $X_{1c}$ level in the barrier (see arrow 2 in Fig. 7a). At this point, the system would switch to a type II alignment with a band gap that is indirect in both real and reciprocal space.

If there is a lattice mismatch between the dot/well and the barrier, e.g., InP/GaP, one has to consider the effects of strain on both the Γ and $X_{1c}$ states in both the well and matrix, in addition to the effects of quantum confinement. These strain effects are illustrated in Fig. 7. In a superlattice, the triply degenerate $X_{1c}$ states in the "well" and the "matrix" layers are split by epitaxial strain into $X_{\|}$ and $X_{\perp}$. The size of the splitting is proportional to the strain which itself is controlled by the relative amounts of matrix and well material. For example, a thick well layer and a narrow barrier layer will produce large epitaxial strain in the barrier and small epitaxial strain in the well. In Fig. 7a, the well layer is thin, resulting in a large epitaxial strain in the well which in turn produces a large splitting of the $X_{1c}$ state in the well. In a strained system, whether the system has a direct or indirect band gap is controlled by two factors: (i) the size of the splitting of the $X_{1c}$ state in the indirect gap matrix, and (ii) the amount of quantum confinement in the direct gap QW. One expects a critical width of QW, below which the effects of quantum confinement push the $\Gamma_{1c}$ derived electron states in the well above the lower of the two split $X_{1c}$ states in the barrier. In this situation, the system has a band gap that is indirect in both real and reciprocal space. If the strain in the barrier is large and hence the splitting of the $X_{1c}$ is large, then less quantum confinement is required to push the $\Gamma_{1c}$ well state above the $X_{1c}$ barrier state. One, therefore, expects the critical width to increase as the well width to barrier width ratio increases and the strain in the barrier increases.

So far we have only considered the strain profile in a two dimensional quantum wells or superlattices. The strain profile of an embedded quantum *dot* is qualitatively different to that of an embedded quantum *well/superlattice*. The strain profile in and around an isotropic *spherical* inclusion embedded in an isotropic matrix was originally derived in 1956 by Eshelby[37] to first order in the lattice mismatch, $\varepsilon_m = (a_i - a_m)/a_m$, where $a_i$ and $a_m$ are the lattice constants of the inclusion and the matrix, respectively. Eshelby showed that inside the sphere, only uniform hydrostatic strain exists,

$$\varepsilon_{in} = \varepsilon_m\left(\frac{1}{\gamma} - 1\right), \tag{8}$$

where $\gamma = 1 + 2B_m(1-2\nu_m)/(B_i(1+\nu_m)$, and where $B_i$ and $B_m$ represent the bulk moduli of the inclusion and the matrix and $\nu_m$ is the Poisson ratio of the matrix. In the

surrounding matrix, however, the strain has both a radial (rad) and tangential (tang) component, given by

$$\varepsilon_{rad}(r) = -2\frac{\varepsilon_m}{\gamma}\left(\frac{R}{r}\right)^3,$$

$$\varepsilon_{tang}(r) = \frac{\varepsilon_m}{\gamma}\left(\frac{R}{r}\right)^3. \quad (9)$$

This *spherical* geometry is unique in that the strain decays as $1/r^3$ with distance r. For lower symmetry geometries such as self-assembled, truncated pyramidal dots, one expects a similar decay of the strain, with however, an additional angular dependence. It is this radial *decay* of the strain away from an embedded dot which is dramatically different to the strain in a quantum well system. In a quantum well or superlattice system the strain is *uniform* throughout both the well and the barrier regions.

States derived from off-Γ points respond in a more complicated fashion to the strain profile described in Eq. (8) and Eq. (9) than the $\Gamma_{1c}$ levels which simply move up and down in response to the hydrostatic strain. A schematic example of one such system is shown in Fig. 7b. In this system, the dot material has a direct gap at the Γ point, while the barrier material has an indirect gap, with the lowest energy conduction state derived from the $X_{1c}$ point (e.g., InP/GaP). The response of the $X_{1c}$ point to the strain profile described in Eq. (8) and Eq. (9) was recently derived by Yang et al.[6] They show that the triply degenerate $X_{1c}$ level is split by the epitaxial strain present at the interface of the dot and the barrier material. This splitting is illustrated in Fig. 7b by the two thin curved lines at the $X_{1c}$ point. In combination with the quantum confinement and strain induced energy level shifts described in the section "Dots Embedded Within a Direct Gap Barrier Material," this splitting of the $X_{1c}$ levels can also induce a type I to type II transition. This transition is illustrated by the two arrows labeled I and 2 in Fig. 7b. In the case where the dot is large, so quantum confinement is small, and the hydrostatic strain induced shift of the $\Gamma_{1c}$ level is also small, absorption will take place from the $\Gamma_{15v}$ hole level to the $\Gamma_{1c}$ electron level in the dot as indicated by arrow 1. However, if the quantum confinement or strain effects are more significant, they can push the $\Gamma_{1c}$ electron level above the lower of the two split $X_{1c}$ levels in the barrier. In this case, electrons will be excited into the interface localized $X_{1c}$ level as indicated by arrow 2, and the system will have an indirect band gap. In this case, the electron state will be localized *at the interface* (see shaded region in Fig. 7b), unlike the quantum well where the X-like electron state is delocalized in the barrier.

## Calculations

*Direct to Indirect transition in dots: GaAs/AlAs*

A common example of a nanostructure with a direct gap, embedded in a barrier material with an indirect gap is the GaAs/AlAs system. As the lattice constants of GaAs and AlAs are almost identical, this system is strain free. Figure 8 shows a set of pseudopotential calculations[38] for GaAs quantum wires with diameters ranging from 0 to 90Å. There is a critical diameter of wire, $d_c$, at which a $\Gamma - X$ crossing takes place in the conduction band of the GaAs wire. Below $d_c$, the lowest energy electron state is derived from the $X_{1c}$ point and is localized in the AlAs matrix.

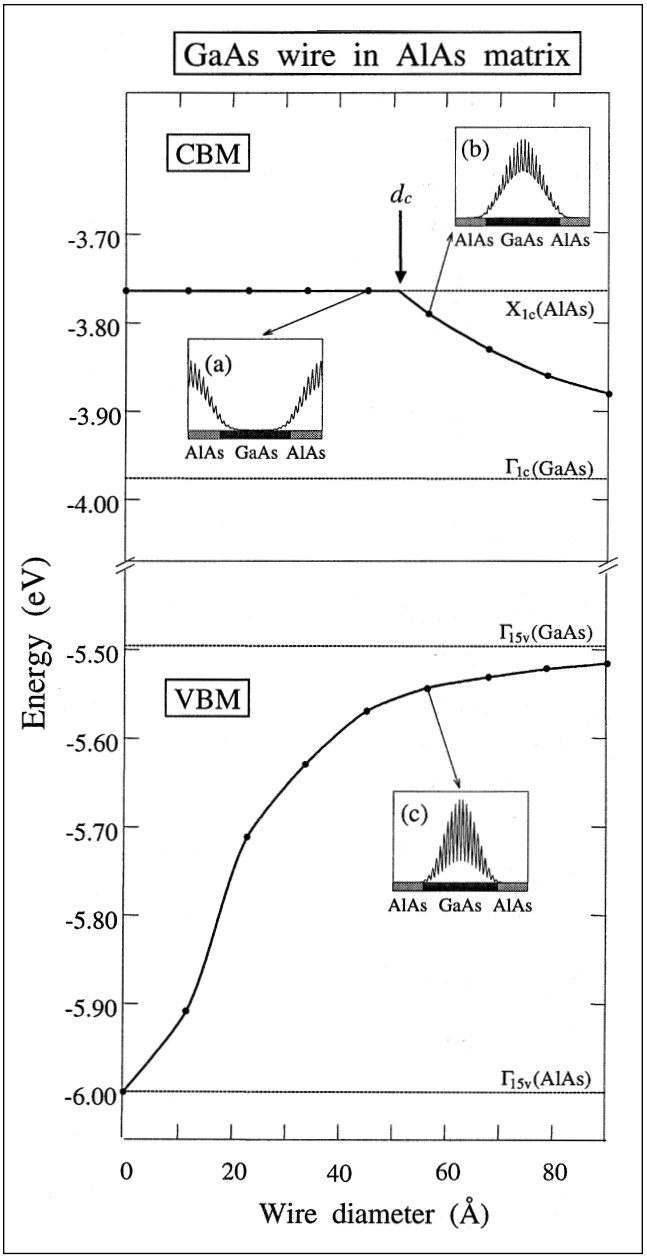


Fig. 8. Pseudopotential calculated[38] VBM and CBM energies of an GaAs cylindrical quantum wire embedded in an AlAs matrix as a function of the wire diameter (solid dots connected by line). The critical diameter for the $\Gamma \rightarrow X$ transition ($d_c$) is indicated by a thick arrow. The dotted lines correspond to the energies of the $\Gamma_{15v}$ and $\Gamma_{1c}$ states of bulk GaAs and of the $\Gamma_{15v}$ and $X_{1c}$ states of bulk AlAs. Insets (a) and (b) show the wavefunction amplitude of the CBM before and after the $\Gamma \rightarrow X$ transition; the CBM amplitude, averaged over the (100) planes (parallel to the wire direction), is plotted along the [100] direction. Inset (c) shows the VBM wavefunction amplitude along the [100] direction.

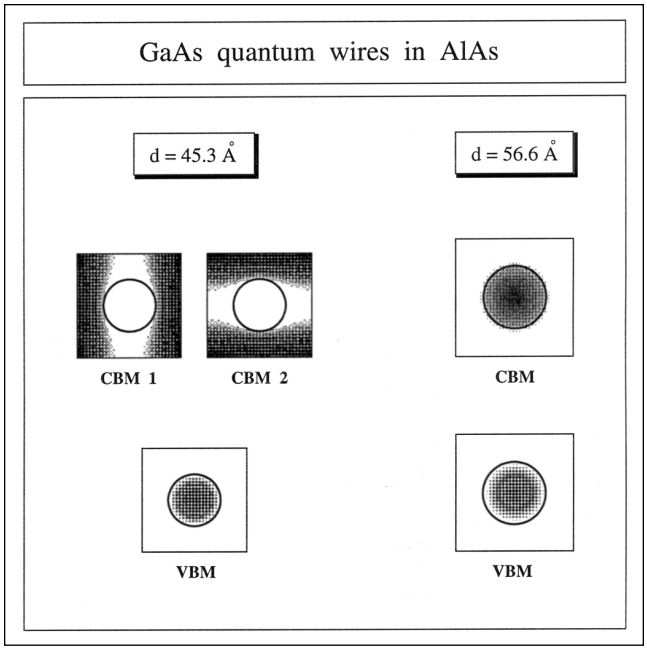


Fig. 9. VBM and CBM wavefunction amplitudes of GaAs [001] quantum wires in AlAs.[38] The wavefunction amplitude, averaged along the wire direction, is plotted in the (001) plane. The solid circles denote cross sections of the GaAs wires (of diameter d). For d = 45.3Å, the CBM is a double-degenerate X-like state localized in the AlAs matrix. For d = 56.6Å, the CBM is a nondegenerate Γ-like state localized in the GaAs wire. In both cases, the VBM is localized in the GaAs wire.

Figure 9 shows the highest energy hole and lowest energy electron states for two AlAs embedded GaAs quantum wires, one with a diameter of 45.3Å (below $d_c$) and one with a diameter of 56.6Å (above $d_c$). Figure 9 shows how the localization of the electron state moves from inside the GaAs wire for diameters above $d_c$ into the AlAs matrix for diameters below $d_c$. Note that for wires with diameters below $d_c$, as the lowest energy electron state is $X_{1c}$ derived, it is, therefore, doubly degenerate. The second line of Table II shows the calculated critical thickness, $l_c$ and critical diameter, $d_c$, for GaAs films and wires embedded in an AlAs matrix.

The above calculations show that quantum wires localize both electrons and holes in the wire for the case of wide quantum wires with a type I alignment. When the wells are narrow and the alignment is type II, charge separation occurs with the electrons localized in the X valley of AlAs and holes are localized in the Γ valley of GaAs. In a recent pseudopotential calculation, Kim et al.[39] showed that for multiple quantum wells with a *curved* geometry charge separation can also occur. However, in their *cylindrical* "Russian Doll" geometry, they show that electron-hole separation can occur on different layers of the same material and the *same* valley. Figure 10 shows the confinement energies and the wavefunction localizations of (a) electrons and (b) holes for a series of concentric cylinder geometries. For each geometry, the inner GaAs cylinder is fixed at 10 ML thick and the surrounding AlAs cylinder is fixed at 4 ML thick. Figure 10 plots the change in localization and confinement energy as the thickness of a third GaAs layer is varied in thickness from 4 to 12 ML. It shows that for a 10:4:10 ratio of GaAs:AlAs:GaAs cylindrical quantum well thicknesses, electrons localize in the Γ valley of the first quantum well layer and holes localize in the Γ valley of the third quantum well layer.

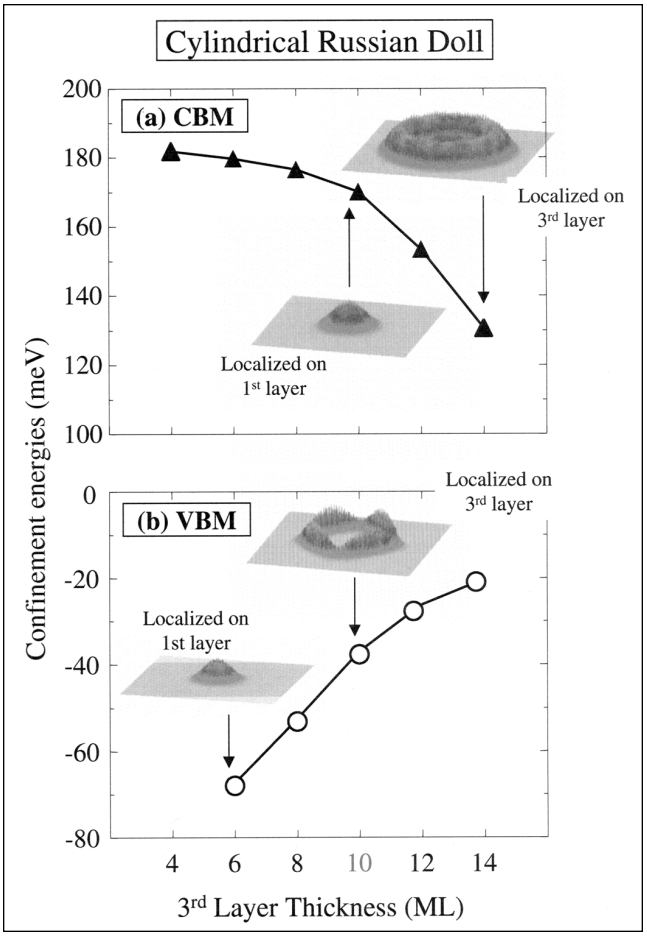


Fig. 10. Confinement energies of the (a) CBM and (b) two highest valence bands for cylindrical Russian Dolls vs the thickness.[39] The other parameters are held fixed at m = 10 ML, n = 4 ML, and q = 8 ML. Wavefunction amplitudes, averaged along the wire direction, are shown as insets for a few structures.

*Direct to Indirect Transition in Quantum Wells: InP/GaP*

The most common example of quantum wells and dots constructed from a direct gap material embedded within a lattice mismatched indirect gap material is InP wells/dots embedded within GaP. Calculations[40] of $(InP)_n(GaP)_n$ (001) superlattices using the LDA as implemented by the all electron, linearized augmented plane wave (LAPW) method[41] predict a quantum confinement induced type I → type II transition occurs as the thickness, n, is decreased below 4.

In Fig. 11, we present the results of empirical pseudopotential calculations performed to test the predictions of Fig. 7a for systems with $n \neq m$ and n, m, > 4. The top of Fig. 11 shows a "phase diagram" indicating which $(InP)_n(GaP)_m$ (001) superlattices have direct and indirect band gaps. Before calculating the

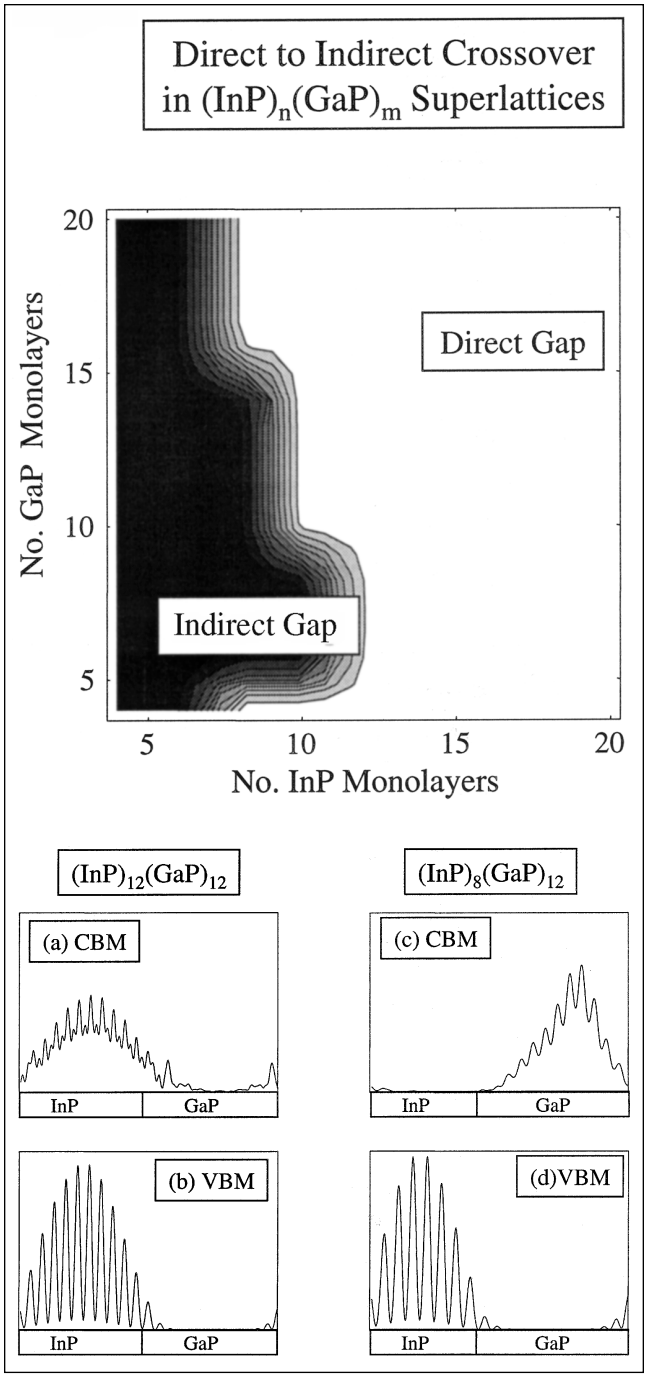


Fig. 11. Pseudopotential calculation[47] of the crossover between direct and indirect gaps in an $(InP)_n(GaP)_m$ superlattice. Figures (a) to (d) show the VBM and CBM wavefunctions squared for an $(InP)_{24}(GaP)_{24}$ superlattice [(a) and (b)] with a direct gap and $(InP)_{16}(GaP)_{24}$ superlattice [(c) and (d)] with an indirect gap.

electronic structure of each superlattice, the atomic positions were first relaxed to their minimum strain energy values, using the valence force field (VFF) elastic energy functional.[42] We see that as predicted in Fig. 7a, as the number of GaP layers increases, the splitting of the $X_{1c}$ derived state in the GaP is reduced, and hence the critical InP well thickness for the direct to indirect transition also decreases. Figures 11a to 11d show two example superlattices with direct and

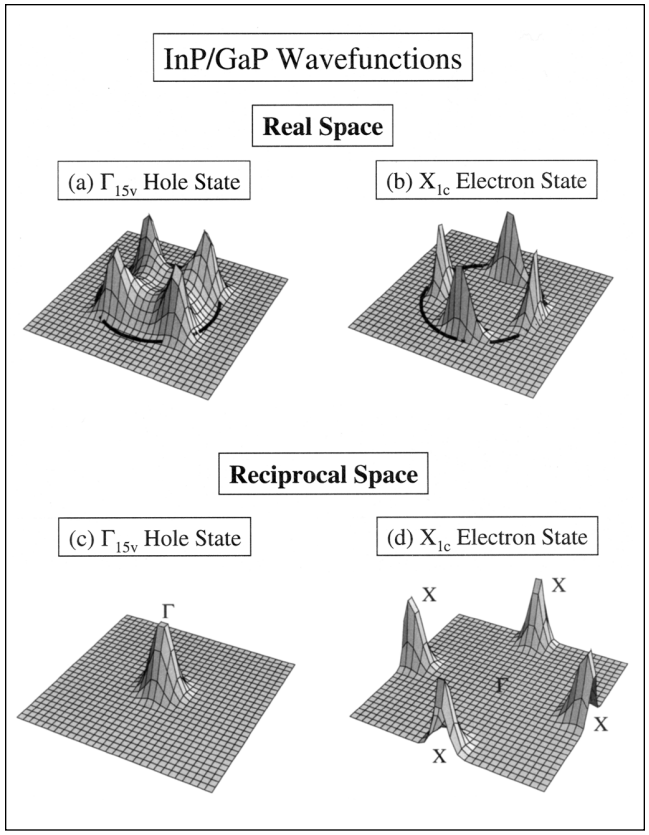


Fig. 12. Wavefunction squared (top) and momentum-space analysis (bottom) for the near edge states of an InP dot with a diameter of 131Å embedded in a GaP matrix. The wavefunctions squared are shown in the (001) plane through the center of the InP dot. The black circles mark the position of the InP/GaP interface. The momentum-space projection of each wavefunction is in the $k_z = 0$ plane of the Brillouin zone.

indirect gaps. Figures 11a and 11b plot the CBM and VBM wavefunctions squared for a $(InP)_{12}(GaP)_{12}$ superlattice. Both the VBM and CBM are localized in the InP region producing a direct gap. Figures 11c and 11d plot the CBM and VBM for a $(InP)_8(GaP)_{12}$ superlattice. Figure 11c shows that the reduction in the width of the InP regime has increased the quantum confinement of the $\Gamma_{1c}$ derived CBM state in the InP, pushing it above the $X_{1c}$ derived state in the GaP and producing an indirect gap.

*Indirect Gap Dots: InP/GaP*

InP quantum *dots* embedded in GaP have been grown[2,43,44] using the Stranski-Krastanow technique and their optical properties have been extensively studied.[43–46] The most recent photoluminescence studies[9] of these dots found almost no emission and the authors conclude that the lowest lying electron state is pushed up by the effects of quantum confinement and strain such that the system is indirect in real and reciprocal space. This result was predicted by recent pseudopotential calculations[47] of spherical InP dots embedded within a GaP matrix. Figure 7b shows that the $X_{1c}$ level is split at the interface of the dot and the barrier, producing an interface localized well for electrons. Figures 12a and 12b show the calculated[47]

amplitude of the electron and hole wavefunctions in a plane through the center of the InP/GaP system. The hole wavefunction is localized within the InP dot as expected, while the electron wavefunction is localized in the strain induced wells, shown as shaded regions in Fig. 7b. To establish the identity of these wavefunctions in terms of the parent GaP and InP bulk states, the dot wavefunctions were projected into the zinc-blende Brillouin zone using the method described in Ref. 48. This mapping is shown in Figs. 12c and 12d for the $\mathbf{k}_z = 0$ plane through the Brillouin zone. We see that the hole state is a Γ-derived state (Fig. 12c), while the lowest conduction state is X-derived (Fig. 12d). The calculated dipole transition matrix element between these states is five orders of magnitude smaller than one would expect between a more typical pair of Γ-derived conduction and valence states, rendering the transition forbidden. This localization of the electrons in a X-derived, interface localized well accounts for the results of Ref. 9.

*Indirect Gap Dots: InAs/GaAs under Pressure > 43 Kbar*

Although, as discussed in the section "Dots Embedded Within a Direct Gap Barrier Material: Calculations: Direct Gap Dots: InAs/GaAs" and Fig. 6, at zero pressure the InAs/GaAs system can be classified as a dot embedded within a direct gap matrix, at a pressure of approximately 43 Kbar[49,50] the GaAs matrix material undergoes a conduction band $\Gamma \rightarrow X$ transition, above which the lowest lying electron state in the GaAs matrix is derived from the $X_{1c}$ point. The system then behaves in a similar manner to that described above for GaP/InP. In Fig. 6, we show the results of pseudopotential calculations[33] for an InAs dot with a base of 100Å and a height of 10Å embedded within a GaAs matrix. The results contrast the lowest lying electron state found at zero and 60 Kbar pressures. Figure 6 shows that at zero pressure, the lowest lying electron state is $\Gamma_{1c}$ derived and localized inside the dot, as discussed in the section "Dots Embedded Within a Direct Gap Barrier Material: Calculations: Direct Gap Dots: InAs/GaAs." However, above the transition pressure, the $X_{1c}$ state in the GaAs barrier is split by the strain at the interface of the dot and the matrix, producing a well for $X_{1c}$ electrons in a similar manner to that discussed above for the GaP/InP system. As a result of this splitting, the lowest lying electron state in the system is $X_{1c}$ derived and localized in a well just above the tip of the pyramid. This predicted switching of the electron state from inside to outside the dot and from the $\Gamma_{1c}$ to $X_{1c}$ point is supported by recent PL experiments.[49,50] These show an increase in the PL energy with pressure up to the critical pressure, P = 43 Kbar. Above the critical pressure, the strength of the PL signal dramatically decreases and the PL energy then decreases with the application of additional pressure. This is the hallmark signature of a Γ – X transition, similar to that predicted in Ref. 33.

*Indirect Gap-Dots:GeSi/Si*

A third example of semiconductor dots embedded within an indirect gap material is that of GeSi dots embedded within Si. This system was analytically studied in Ref. 6. The authors predict that for all Ge compositions, x, of a spherical $Ge_xSi_{1-x}$ dot embedded within a Si matrix, the band alignment will be type II and the system will have an indirect band gap. They also use finite element calculations to demonstrate that the approximation of an *isotropic* inclusion in an *isotropic* matrix, adopted in Eq. (8) and Eq. (9), alters the band energies by less than 0.01 eV.

## CONCLUSIONS

We have classified semiconductor quantum dots into three categories; (i) free standing dots, (ii) dots embedded in a direct gap matrix, and (iii) dots embedded in an indirect gap matrix.

- Free standing dots may have (i) a direct gap for all experimental sizes (e.g., InAs, InP, and CdSe) or (ii) if the initial conduction band level spacing is small and the effects quantum confinement are strong enough, they may switch to an indirect gap below a critical diameter (e.g., GaAs and InSb).
- Dots embedded in a direct gap material may have (i) a direct gap (e.g., InAs/GaAs) if the natural conduction band offset between the dot and the matrix is type I. However, (ii) even if the offset is type I, the dots may still switch to an indirect gap if either quantum confinement or strain effects push the $\Gamma_{1c}$ level in the dot above that of the matrix (e.g., InSb/InP).
- Dots embedded in an indirect gap material can be classified into two groups; (i) GaAs/AlAs undergoes a direct to indirect transition below a critical size. (ii) InAs/GaAs above 43 kbar pressure, InP/GaP and GeSi/Si all have type II band alignments and indirect gaps for all sizes.

Finally, we show that a result of the different strain profiles in quantum dot and quantum well systems, one does not see the interface localized states observed in certain quantum dot systems occur in quantum well systems constructed from the same materials (e.g., InP/GaP).

## ACKNOWLEDGMENTS

This work was supported DOE-Basic Energy Sciences, Division of Materials Science under contract No. DE-AC36-83CH10093.

## REFERENCES

1. N. Stranski and L. Krastanow, *Math.-Naturwiss Kl.* Abt. IIb 146, 797 (1938).
2. N. Carlsson et al., *Appl. Phys. Lett.* 66, 3093 (1994).
3. K. Schmidt, G. Medeiros-Ribeiro, M. Oestreich and P. Petroff, *Phys. Rev. B* 54, 11346 (1996).

4. G. Solomon, J. Trezza, A. Marshall and J. Harris, *Phys. Rev. Lett.* 76, 952 (1996).
5. J. Prieto, G. Armelles, T. Utzmeier, F. Briones, F.C. Ferrer, F. Peiro, A. Cornet and J.R. Morante, *Phys. Rev. Lett*. 80, 1094 (1998).
6. M. Yang, J. Sturm and J. Prevost, *Phys. Rev. B* 56 1973 (1997).
7. M. Reed. *Phys. Rev. Lett.* 60, 5353 (1988).
8. R. Leon, C. Lobo, T.P. Chin, J.M. Woodall, S. Fofard, S. Ruvimov, Z. Liliental-Weber and M.A. Steven-Kalceff, *Appl. Phys. Lett.* 72,1356 (1998).
9. B. Junno, T. Junno, M. Miller and L. Samuelson, *Appl. Phys. Lett* 72, 954 (1998).
10. O. Micic, C. Curtis, K. Jones, J. Sprague and A. Nozik, *J. Phys. Chem*. 98, 4966 (1994).
11. S. Empedocles, D. Norris and M. Bawendi, *Phys. Rev. Lett*. 77, 3873 (1996).
12. A. Guzelian, U. Banin, A. Kadavanich, X. Peng and A. Alivisatos, *Appl. Phys. Lett.* 69, 1432 (1996).
13. A. Colvin, V.L.and Alivisatos and J. Tobin, *Phys. Rev. Lett.* 66, 2786 (1991).
14. Landolt and Börnstein, *Numerical Data and Functional Relationships in Science and Technology*, Vol. 22, Subvol. a (Berlin: Springer-Verlag, 1997).
15. A. Williamson, J. Kim, L.-W. Wang, S.-H. Wei and A. Zunger, unpublished results.
16. C. Pryor, J. Kim, L.-W. Wang, A. Williamson and A. Zunger, *J. Appl. Phys.* 83, 2548 (1998).
17. L.-W. Wang and A. Zunger, *Phys. Rev B.* 51, 17398 (1995).
18. L.-W. Wang and A. Zunger, *J. Chem. Phys.* 100, 2394 (1994).
19. L.W. Wang and A. Zunger, *Semiconductor Nanoclusters* (Amsterdam: Elsevier Science, 1996).
20. A. Franceschetti and A. Zunger, *Appl. Phys. Lett.* 68, 3455 (1996).
21. A. Franceschetti and A. Zunger, *J. Chem. Phys.* 104, 5572 (1996).
22. H. Fu and A. Zunger, *Phys. Rev. B* 55, 1642 (1997).
23. H. Fu and A. Zunger, *Phys. Rev. B* 56, 1496 (1997).
24. H. Fu and A. Zunger, *Phys. Rev. B* 57, R15067 (1998).
25. H. Fu, L.-W. Wang and A. Zunger, *Phys. Rev. B* 57, 9971 (1998).
26. H. Fu and A. Zunger, *Phys. Rev. Lett*. 80, 5397 (1998).
27. A. Williamson and A. Zunger, *Phys. Rev. B* Code: BY6599 (1998).
28. L.-W. Wang and A. Zunger, *J. Phys. Chem.* 102, 6449 (1998).
29. L.-W. Wang and A. Zunger, *Phys. Rev B* 53, 9579 (1996).
30. U. Banin et al., *J. Chem. Phys.* (in press) (1998).
31. D. Bertram, O. Micic and A. Nozik, *Phys. Rev. B* 57, R4265 (1998).
32. S. Tolbert, A. Herhold, L. Brus and A. Alivisatos, *Phys. Rev. Lett.* 76, 4384 (1996).
33. A. Williamson and A. Zunger, *Phys. Rev. B* 48, 6724 (1998).
34. J. Kim, L.-W. Wang and A. Zunger, *Phys. Rev. B* 57, R9408 (1998).
35. A. Zunger, *MRS Bulletin* 23, 35 (1998).
36. G. Griffiths, K. Mohammed, S. Subbanna, H. Kroemer and J. Merz, *Appl. Phys. Lett*. 43, 1059 (1983).
37. J. Eshelby, *J. Appl. Phys.* 25, 255 (1954).
38. A. Franceschetti and A. Zunger, *Phys. Rev. B* 52, 14664 (1995).
39. J. Kim, L.-W. Wang and A. Zunger, *Phys. Rev. B* 56, R15541 (1997).
40. A. Franceschetti, S.-H. Wei and A. Zunger, *Phys. Rev. B Rapid Commun*. 50, 8094 (1994).
41. S.-H. Wei and H. Krakauer, *Phys. Rev. Lett.* 55, 1200 (1985).
42. P. Keating, *Phys. Rev.* 145, 637 (1966).
43. C. Ulrich et al., *Phys. Rev. B* 52, 12212 (1995).
44. T. Okuno et al., *Phys. Rev. B* 57, 1386 (1998).
45. M. Pistol, N. Carlsson, W. Persson, C. and Seifert and L. Samuelson, *Appl. Phys. Lett* 67, 1438 (1995).
46. P. Castrillo et al., *Appl. Phys. Lett* 67, 1905 (1995).
47. A. Williamson, A. Zunger and A. Canning, *Phys. Rev. B* 57, R4253 (1997).
48. L.-W. Wang and A. Zunger, *Phys. Rev B* 56 (1997).
49. G. Li, A. Goni, K. Syassen, O. Brandt and K. Ploog, *Phys. Rev. B* 50, 18420 (1994).
50. I. Itskevich et al., *Phys. Rev. B* 54, 16401 (1996).